STRUCTURAL DETERMINANTS UNDERLYING PHOTOPROTECTION IN THE PHOTOACTIVE ORANGE CAROTENOID PROTEIN OF CYANOBACTERIA

Adjele Wilson[1,2], James N. Kinney[3], Petrus H. Zwart[3], Claire Punginelli[1,2], Sandrine D'Haene[1,2], François Perreau[4], Michael G. Klein[3], Diana Kirilovsky[1,2] and Cheryl A. Kerfeld[3,5]

From Commissariat à l'Energie Atomique (CEA), Institut de Biologie et Technologies de Saclay (iBiTec-S) [1] and Centre National de la Recherche Scientifique (CNRS), URA 2906, 91191 Gif sur Yvette, France,[2] United States Department of Energy - Joint Genome Institute, Walnut Creek CA 94598,[3] Institut Jean-Pierre Bourgin, UMR 1318 INRA-AgroParisTech, INRA Versailles-Grignon, Route de Saint Cyr, F-78026 Versailles, France[4] and Department of Plant and Microbial Biology, University of California, Berkeley, CA 94720[5]

Address correspondence to: Cheryl Kerfeld UCB/JGI, 2800 Mitchell Drive, Walnut Creek, CA 94598. Tel.: 925-296-5691; FAX 925-296-5752; E-mail: ckerfeld@berkeley.edu

Running title: Structural Insights into Cyanobacterial Photoprotection

The photoprotective processes of photosynthetic organisms involve the dissipation of excess absorbed light energy as heat. Photoprotection in cyanobacteria is mechanistically distinct from that in plants; it involves the Orange Carotenoid Protein (OCP), a water-soluble protein containing a single carotenoid. The OCP is a new member of the family of blue light photoactive proteins; blue-green light triggers the OCP-mediated photoprotective response. Here we report structural and functional characterization of the wildtype and two mutant forms of the OCP, from the model organism *Synechocystis* PCC6803. The structural analysis provides high resolution detail of the carotenoid-protein interactions that underlie the optical properties of the OCP, unique among carotenoid-proteins in binding a single pigment per polypeptide chain. Collectively, these data implicate several key amino acids in the function of the OCP and reveal that the photoconversion and photoprotective responses of the OCP to blue-green light can be decoupled.

The capture of light energy for oxygenic photosynthesis is arguably one of the most important metabolic processes on earth. It is also inherently risky; the absorbance of excess light energy beyond what can be used in photosynthesis can result in photooxidative damage to the organism. Consequently, photosynthetic organisms have evolved protective mechanisms to dissipate excess captured energy. In plants, one of these mechanisms involves the membrane-embedded chl antenna of Photosystem II (PSII), the Light-Harvesting-Complex (LHCII) (for reviews, see (1-4). Under saturating light conditions, the decrease of the lumen pH activates the xanthophyll cycle (5,6) and the protonation of PsbS, a PSII subunit (7). Conformational changes in the LHCII, modifying the interaction between chlorophyll molecules and carotenoids and allowing thermal dissipation, are also involved in this mechanism (8-10). Energy dissipation is accompanied by a diminution of PSII related fluorescence emission, also known as non-photochemical-quenching (NPQ; more specifically qE) which usually serves as a measure of the dissipation process.

While the photoprotective mechanism of plants is well studied, only recently have

mechanisms for photoprotection in the cyanobacteria been discovered (11-17). One of these occurs at the water-soluble light harvesting antenna (the phycobilisome), and involves a novel photosensory protein, the Orange Carotenoid Protein (13, 18-20). Most cyanobacterial species contain the OCP (21,22) and in these organisms it is constitutively expressed and is also upregulated under extreme conditions such as high light, iron starvation and salt stress (18,23-25). The OCP-mediated photoprotective mechanism is completely distinct from any known in plants and algae; it involves the absorption of blue-green light which induces a shift in the absorbance properties of the OCP; visibly the protein changes from orange to red (photoconversion). The structural basis of this photoconversion is unknown, but it appears to be a result of changes in both the protein and the carotenoid (19). The red, photoactive form of the protein induces the dissipation of energy from the phycobilisome as heat. This results in a measurable decrease (quenching) of phycobilisome fluorescence known as nonphotochemical quenching.

The OCP is of particular interest because it is the only photosensory protein characterized to date that uses a carotenoid as the chromophore. More broadly speaking, it is also a new member of the family of blue light photoactive proteins; blue-green light is a ubiquitous environmental signal that activates a functionally diverse range of bacterial proteins such as Photoactive Yellow Protein (PYP; (26,27)) and those containing LOV (28-31) or BLUF domains (32-35). Recent data available from genome sequencing as well as structural and functional characterization of these sensory proteins and their relatives has revealed that they share some general features in the structural basis of photoresponsiveness and signal transduction (36,37).

Because the OCP is one of the few examples of a carotenoid-binding protein that is water soluble and that contains only a single carotenoid molecule per polypeptide chain, it is an ideal system for the study of carotenoid-protein interactions. Mutant forms of the OCP, which can be made in *Synechocystis* PCC 6803 (hereafter, *Synechocystis*), enable dissection of the role of individual amino acids in binding and in tuning the spectral properties of the carotenoid as well as their role in photoconversion and photoprotection. The 2.1 Å crystal structure of the OCP, from *Arthrospira maxima*, was reported in 2003, prior to an understanding of its function (38). Subsequent studies of the OCP in the model organism *Synechocystis* revealed its role in photoprotection (13,18,19). Here we report the 1.65 Å crystal structure of the WT-OCP and of two OCP mutants from *Synechocystis*. The structural and functional characterization of OCP point mutants identified key roles for specific amino acids (W110, Y44 and R155) and demonstrated that the processes of photoconversion and nonphotochemical quenching can be decoupled. In addition, comparison of the *Synechocystis* and *A. maxima* OCP structures enabled identification of structurally conserved water molecules that may play a functional role. Finally, multiple structures of the OCP considered in the context of structure-function studies of other blue-light photoactive proteins reveal some interesting parallels and inform new hypotheses about the structural basis of the OCP's photoprotective function.

EXPERIMENTAL PROCEDURES

Culture conditions—Synechocystis wildtype and mutants were grown photoautotrophically in a modified BG11medium (39) containing twice the amount of sodium nitrate. Cells were kept in a rotary shaker (120 rpm) at 30°C, illuminated by fluorescent white lamps giving a total intensity of about 30–40 μmol photons m^{-2} s^{-1} under a CO_2-enriched atmosphere. The cells were maintained in the logarithmic phase of growth and were collected at OD800 nm=0.6–0.8. For OCP isolation, *Synechocystis* cells were grown in 3L Erlenmeyer flasks in a rotary shaker under a light intensity of 90–100 μmol photons m^{-2} s^{-1}. The cells were harvested at an OD800 nm=0.8-1.

Construction of OCP Synechocystis mutants-- To obtain single OCP mutants, wildtype *Synechocystis* cells were transformed by a plasmid containing the mutated OCP gene (*slr1963*) with a C-terminal His-tag, and the hypothetical gene *slr1964* interrupted by a spectinomycin and streptomycin (Sp/Sm) resistance cassette (9). The point mutations Y44S, Y44F, W110F and R155L were obtained by changing one or two nucleotides in the *slr1963* gene by site-directed mutagenesis using the Quickchange XL site-directed mutagenesis kit (Stratagene) and synthetic

oligonucleotides (all of the oligonucleotides used in this work are described in Supp Table 1). To obtain double OCP mutants overexpressing the mutated OCP, the mutated *slr1963* gene was cloned in an overexpressing plasmid in which the *slr1963* gene is under the control of the *psbAII* promoter. The construction of the plasmid was described in (19). The plasmids containing the mutated *slr1963* genes under the control of the *psbAII* promoter were used to transform single OCP mutants of *Synechocystis* by double recombination (Supp. Fig 1).

To confirm the introduction of the different mutations in the genomic *Synechocystis* DNA and complete segregation of mutants, PCR analysis and digestion by specific restriction enzymes were performed. Supp. Fig. 2*A* shows that amplification of the genomic region containing the *slr1963* and *slr1964* genes (in the *psbAII* locus (lanes 1-4) or in the *slr1963* locus (lanes 5-9) using the synthetic psba1 and psba2 oligonucleotides or car6 and car7 oligonucleotides gave fragments of 1.5 kb or 2.2 kb respectively in the wildtype and of 3.5 kb and 4.3 respectively in the mutants containing the antibiotic cassettes. No traces of the wildtype fragment were detected in the mutants indicating complete segregation. The presence of the different mutations was detected by digestion with restrictions enzymes (Supp. Figs. 2*B* and 2*C*). The presence of the Y44S and W110F mutation was confirmed by the appearance of the supplementary NheI restriction site and the disappearance of the KpnI restriction site respectively. Digestion of the amplified DNA fragments by BsmI indicated the presence of the R155L mutation. The presence of the mutations was confirmed by DNA sequencing.

The construction of the His-tagged OCP, the overexpressing His-tagged OCP, His-tagged W110S OCP and the overexpressing His-tagged W110S OCP were described in (19).

Purification of the Orange Carotenoid Protein-- The purification of *Synechocystis* OCP was performed as previously described (19). Briefly, mutant cells (1 mg Chl ml^{-1}) in Tris-HCl pH=8 buffer were broken in dim light using a French Press. The membranes were pelleted and the supernatant was loaded on a column of Ni-Probond resin (Invitrogen). The OCP was further purified on a Whatman DE-52 cellulose column. Additional details of the purification are described in (19). The protein was stored in the dark at 4°C.

Absorbance and fluorescence measurements-- Cell absorbance was monitored with an UVIKONXL spectrophotometer (SECOMAN, Alès). Chlorophyll content was determined in methanol using the extinction coefficient at 665 nm of 79.24 mg mL^{-1} cm^{-1}. The orange to red photoconversion was monitored in a Specord S600 (Analyticjena, France) spectrophotometer during illumination of the OCP with 1200 µmol photons m^{-2} s^{-1} of blue-green light (400–550 nm) at 12 °C. Cell fluorescence was monitored with a pulse amplitude modulated fluorometer (101/102/103-PAM; Walz, Effelrich, Germany). All measurements were carried out in a stirred cuvette of 1 cm diameter at growth temperature (32 °C). Cells were pre-adapted to low irradiance of blue-green light (400–550 nm, 80 µmol photons m^{-2} s^{-1}) for about 1 min; then, fluorescence quenching was induced by 740 µmol photons m^{-2} s^{-1} of blue-green light for about 200 s. Saturating pulses (2000 µmol photons m^{-2} s^{-1}) were applied to measure the maximal fluorescence levels, Fm', in light-adapted samples,. Application of such pulses that transiently close all the Photosystem II centers serves to distinguish between photochemical quenching and non-photochemical quenching.

OCP Immunodetection--Total cell protein was analyzed by SDS-PAGE on a 12% polyacrylamide/2 M urea (Supp. Fig. 3) in a TRIS/MES system (40). The OCP protein was detected by a polyclonal antibody against OCP (18).

Carotenoid characterization—Carotenoids were extracted from OCP proteins as previously described (41). Liquid chromatography-mass spectrometry analysis was performed as described in (42).

Sequence Analysis-- The OCP logo was produced using an alignment of 28 OCP orthologs (reciprocal best BLAST hits to *Synechocystis* OCP) generated in Tcoffee (http://www.ebi.ac.uk/Tools/t-coffee/index.html). The hmmer package of tools on the Mobyle server at http://mobyle.pasteur.fr were used to generate an HMM from the alignment. The HMM was built using hmmbuild and then calibrated using hmmcalibrate. The LogoMat-M server at http://www.sanger.ac.uk/cgi-

bin/software/analysis/logomat-m.cgi was used to generate the HMM logo from the HMM.

Crystallization and structure determination- Wildtype and mutant *Synechocystis* OCP were crystallized at 18 ºC by the hanging drop vapor diffusion method over reservoir solutions identified from a screen of >1000 crystallization conditions. Because of the lack of appreciable effect of ambient light in triggering photoconversion of the OCP, no special precautions were taken to avoid room light. Wildtype OCP (3.8 mg/ml 10 mM Tris pH 7.7) was crystallized in drops containing 2ul of protein plus 1 ul reservoir solution (100 mM sodium acetate, pH 5.0, 10 % PEG8,000). Y44S OCP (3.3 mg/ml 10 mM Tris pH 7.7) was crystallized in drops containing 2ul of protein and 1ul of reservoir solution (0.2M CaCl2, 18 % PEG3350). R155L OCP (2.6 mg/ml 10 mM Tris pH 7.7) was crystallized in drops containing 2ul of protein plus 0.5 ul reservoir solution (100 mM sodium acetate pH 5.0, 10 % PEG 3350 and 2% glycerol). Protein concentration was measured using the Bradford protein assay (Bio-Rad).

For data collection, crystals were rapidly transferred into reservoir solutions supplemented with 25% glycerol, mounted into nylon loops, and frozen by placing directly into the cryo-stream of nitrogen gas. Diffraction data were collected at Lawrence Berkeley's Advanced Light Source, beamlines 8.2.1 and 5.02. The diffraction data were integrated and scaled with DENZO and SCALEPACK using HKL2000 (43). The wildtype and both OCP mutants crystallized in space group $P3_2$ with two molecules in the asymmetric unit.

Structures were solved by molecular replacement using PHASER (44) implemented in CCP4 (45), and refinement was performed with phenix.refine (46) and REFMAC5 (47) using iterative cycles of positional, and atomic B-factor refinement, and model building with 2Fo-Fc and Fo-Fc maps in COOT (48). During the final stages of refinement, NCS restraints were released in the structures of the wild type and R155L mutant, to allow for slight differences in the monomers. TLS refinement was performed for the wildtype and R155L structures; Four TLS domains were chosen using the TLSMD server (http://skuld.bmsc.washington.edu/~tlsmd/) corresponding to residue ranges 4-72, 73-169, 170-243 and 244-320.

In all three structures there was some disorder at the N- and C-termini and in the linker region between the two domains, so these regions were not modelled. The refined wild type OCP structure (1.65 Å resolution) contains residues 3-164 and 171 to 312 (chain A), and residues 3-164 and 171 to 312 (chain B). The Y44S mutant OCP (2.65 Å resolution) contains residues 4-163 and 172-312 (chain A), and residues 4-163 and 171-312 (chain B). The R155L mutant OCP (1.70 Å) contains residues 4-164 and 170-312 (chain A), and residues 3-164 and 170 to 312 (chains B). Electron density maps for each of the three models were well featured for the echinenone (ECN), enabling modelling at the final stages of refinement. Alternate conformations for sidechains were visible in the relatively high resolution wildtype and R155L models; these we modelled manually. Waters were modelled using the automatic solvent detection function in phenix.refine and checked manually in COOT. Additional crystallography statistics are listed in Table 1.

Analysis of the structures--The stereochemistry of the final refined models were analyzed by MolProbity (49). Least squares RMS deviation for comparison of different structures was performed with LSQKAB (50). Protein interfaces were analyzed using PDBSUM (51), PISA (52) and Profunc (53) servers at the European Bioinformatics Institute. Intraprotein aromatic-sulfur and aromatic aromatic interactions were identified with the Protein Interaction Calculator (54) and protein-carotenoid interactions defined by LigPlot (55). Figures were prepared with PyMol (56).

The atomic coordinates and structure factors (3I1V, wildtype; 3I1W, Y44S mutant; 3I1X, R155L) have been deposited in the Protein Data Bank, Research Collaboratory for Structural Bioinformatics, Rutgers University, New Brunswick, NJ (http://www.rcsb.org/).

Conserved waters in the Synechocystis and Arthrospira OCP structures-- Structurally conserved water molecules were identified after superimposing the structures in the graphics program O (57), and then identifying overlapping waters within a 0.7Å cut-off.

Size Exclusion Chromatography--Purified *Synechocystis* OCP was injected to a Superdex 75 HR 10/30 column (Pharmacia) equilibrated with 40 mM Tris-HCl pH 8, 150 mM NaCl. The Akta FLPC system is equipped with a UV detector at 280 nm and was running at a flow

rate of 0.5 ml/min. The gel filtration standard (Biorad) included thyroglobulin (670 kDa), bovine gamma-globulin (158 kDa), chicken ovalbumin (44 kDa), equine myoglobin (17 kDa) and bovine serum albumin (66 kDa). The standards were separated under the same conditions with and without OCP.

RESULTS AND DISCUSSION

Purification and Carotenoid Content of Wildtype and Mutant OCP. For purification of the OCP for structural and functional studies, His-tagged overexpressing OCP mutant strains of *Synechocystis* were constructed. The expressed protein was purified by Ni-affinity and ion-exchange chromatography (19). Analysis of the carotenoid content of the mutant proteins revealed that they contained a mixture of 3'-hydroxyechinenone, echinenone (ECN) and zeaxanthin (Table 2; Supp. Fig. 4), as previously observed in strains overexpressing WT-OCP (42). The relative content of each carotenoid varied depending on the quantity of OCP present in the cell and on the mutation. With the exception of the OCP with a modified Trp^{110}, in which 3'hydroxyechinenone was the principal carotenoid detected, echinenone was the most abundant carotenoid present in OCP isolated from overexpressing strains. The presence of zeaxanthin varied from 6 to 30%. In darkness or dim light, the OCP isolated from all of the mutant strains appeared orange and their absorption spectra were only slightly different (Fig. 1). In some mutants (especially Y44S-OCP), a spectrally distinct small fraction containing more zeaxanthin eluted at slightly lower salt concentration suggesting that the zeaxanthin-containing OCP detached more easily from the ion-exchange column (data not shown). The zeaxanthin-OCP being inactive (42), this fraction was not used for further studies. Upon illumination with blue-green light, the WT OCP (containing only 3'-hydroxyechinenone (Table 2) was completely photoconverted to a red form (absorption maxima at 500-510 nm) while the OCP isolated from the overexpressing strain (containing 14% zeaxanthin) was not completely photoconverted (absorption maximum 498 nm) (Fig 1 and (42)).

Structure of Synechocystis OCP. The structure of wildtype *Synechocystis* OCP was solved by molecular replacement using a monomer of the *Arthrospira maxima* OCP (38) as a search model and refined to 1.65Å with a final *R*/*R*free of 16.2/19.1%. The *Synechocystis* OCP was then used as a search model in molecular replacement to solve the crystal structures of the R155L and Y44S *Synechocystis* OCP mutants at 1.7Å and 2.7Å resolution, respectively. Data and refinement statistics are given in Table 1.

The OCP consists of two domains (Fig. 2*A*), an N-terminal helical domain (residues 19-165; Pfam09150), composed of two four-helix bundles. The N-terminal domain of the OCP is the only known example of this protein fold. In contrast, the C-terminal domain (residues 193-311) is a member of the nuclear transport factor 2 (NTF2) superfamily (Pfam02136), which is found in a wide range of organisms. The NTF2 domain is a mixed alpha/beta fold: in the OCP it comprises a five stranded beta sheet core flanked by three alpha helices, (αK, αL, αM). The N- and C-terminal domain are joined by a 28 amino acid linker that is the most variable region of primary structure among OCP orthologs (Fig. 3). Because of disorder, the first several residues of the linker (~164-171) could not be modelled in any of the three structures, suggesting that the region is flexible. The *Synechocystis* OCP structure closely resembles that of *A. maxima* (superimposing with a r.m.s. deviation of 0.55Å over 301 alpha carbon atoms), reflecting the similarity (83% identical) of their primary structures. Indeed, the primary structure of all OCP orthologs is strongly conserved (21).

The three *Synechocystis* OCP structures were also similar to that of *A. maxima* OCP in that each contained two molecules in the crystallographic asymmetric unit arranged as an approximate antiparallel dimer (Fig. 4*A*). The dimerization interface in all four structures is similar, involving mainly the N-terminal domain. It contains 14 hydrogen bonds, two salt bridges (between Arg^{27} and Asp^{19}) and two water molecules that are conserved in both the *A. maxima* and *Synechocystis* OCP structures. The amount of surface area buried in the dimerization, ~1100 $Å^2$/monomer, exceeds the threshold value proposed to discriminate between a presumably biologically relevant interface and a crystal contact (856 $Å^2$, (58)). Because of the repeated observations of this interface in the different OCP structures, its size and the

precedent for functionally relevant oligomeric state changes in other blue light responsive proteins (33,59), we considered the likelihood that the OCP dimer is functionally relevant. The *A. maxima* OCP has been reported to be a dimer in gel filtration (38). However, *Synechocystis* OCP eluted as a monomer in gel filtration in both its resting (orange; Fig. 5) and photoactivated form (data not shown). Moreover, thermodynamic calculations of the energy of binding of the intermolecular interface in both the *A. maxima* and *Synechocystis* dimers suggest it is not a stable assembly. Furthermore, if the OCP dimer was functionally relevant, it would be expected that residues in the intermolecular interface would be conserved in the primary structure of the OCP; however, only three of the 22 amino acids making up the dimerization interface are absolutely conserved among OCP orthologs. It appears more likely that the repeatedly observed dimerization in the crystals is an artifact of the relatively high protein concentration and/or conditions used for crystallization.

Structural Parallels to Other Blue-light Photoreceptor Proteins. In the past five years while we have gained an understanding of the function of the OCP, a substantial amount of new structural, functional and sequence information has been obtained for other blue light photoreceptors such as BLUF and LOV domains and PYP (which, like the LOV domain, is a member of the PAS structure superfamily). BLUF and LOV domains are found covalently connected to their effector domains, or can be present as isolated modules with the their effector domains encoded separately. Interestingly, common mechanistic principles underlying response to blue-green light in PYP and the functionally diverse BLUF and LOV domains are emerging (36). LOV and BLUF domains as well as PYP share a common beta sheet core flanked by helices. The interaction of the chromophore with the beta sheet originates a signal that is propagated to the effector region of the protein through sidechain movements and changes in hydrogen bonding patterns. The OCP is similar to these other blue-light responsive proteins in that the core of its C-terminal domain, which hydrogen bonds to the carotenoid, is a beta sheet flanked by helices. Likewise, accumulating genomic sequence data suggests that modularity is part of the evolutionary history of the OCP; open reading frames encoding isolated N- and C-terminal domains of the OCP are observed in numerous cyanobacterial genomes (21). Accordingly, in interpreting the specific features of the OCP structure in the context of function we consider if there is evidence of structural features similar to those that underlie the general principles of signal transduction known from PYP and BLUF and LOV domains.

Carotenoid-Protein Interactions in the Synechocystis OCP and Implications for Function. The OCP isolated directly from *A. maxima* and *Synechocystis* cultures contains the carotenoid 3'hydroxyechinenone, while the *Synechocystis* mutant overexpressing the OCP contains mainly ECN (Table 2; (42)); the photoprotective activity of the ECN-containing OCP is comparable to that containing 3'-hydroxyechinenone, indicating that the hydroxyl group in 3'-hydroxyechinenone, which potentially hydrogen bonds to the N-terminal domain in the *A. maxima* OCP, is not critical for function (42) Electron density maps calculated using phases from the partially refined model of the *Synechocystis* OCP without carotenoid were of high quality, enabling *de novo* building of the ECN molecule in each monomer. The conformation of the ECN in the two *Synechocystis* OCP monomers is identical (within the range of coordinate error) and are similar to that of 3'-hydroxyechinenone in the *A. maxima* OCP (r.m.s deviation 0.2 Å over 41 atoms; Fig 4*B*). As in the *A. maxima* OCP, the carotenoid in the *Synechocystis* OCP spans the N- and C-terminal domains; it is almost entirely buried; only 4% of the ECN is solvent exposed. In the N-terminal domain, the ECN is nestled between the two four-helix bundles (Fig. 2*A*). In the C-terminal domain, it occupies a cleft formed between the beta sheet and αM and αK (Figs. 2*B* and 4*A*). The keto group of the ECN hydrogen bonds with the absolutely conserved amino acids Tyr201 (αY) and Trp288 of the central strand (β4) of the beta sheet (Fig. 2*B*); the H-bonding distance are 2.6Å and 2.9Å, respectively. The H-bond to Tyr^{201} is a relatively short hydrogen bond, which are often functionally important (60,61). Short hydrogen bonds between the chromophore and the protein are the basis of a network of hydrogen bonds in PYP that are critical to its

photocycle (62). In the OCP, the orientation of the Tyr^{201} sidechain appears to be stabilized via aromatic interactions (63), with two absolutely conserved phenylalanine sidechains (217 and 290), while the orientation of Trp^{288} may be in part stabilized by an aromatic sulfur interaction with the strongly conserved Met^{202} . The importance of the hydrogen bonds between the protein and the carotenoid for the function of the OCP is underscored by studies of zeaxanthin-containing OCP; zeaxanthin lacks an oxygen atom for hydrogen bonding and zeaxanthin-OCP is not photoactive, nor is it able to induce fluorescence quenching under strong blue-green light (42). Changes in these hydrogen bonds upon photoactivation could be communicated through the beta sheet or to the surface of the OCP via residues hydrogen bonded to Tyr^{201} and Trp^{288} (Fig. 2*B*). For example, the backbone of Tyr^{201} is hydrogen bonded to the backbone of Thr^{197} (αK) which is surface exposed. Through backbone atoms, Tyr^{201} is hydrogen bonded (3.1Å) to Leu^{205} (αK), which is hydrogen bonded (3.0Å), also through backbone atoms, to surface exposed Asn^{208}. The backbone of Trp^{288} (β4) forms two hydrogen bonds to the backbone of Val^{269} (β3; 2.8Å and 2.9Å). Through an aromatic – sulfur interaction with Met^{202} and its hydrogen bonding, Trp^{288} has additional communication to the αK helix. The multiple hydrogen bonding pathways to the αK helix are notable because it is part of the C-terminal domain in the OCP (αK, β2, β3, β4) that shows some structural similarity to the phycobilisome core linker protein, APLc (19); mimicking the interaction of the linker with the phycobilisome core could allow this region to interact with the chromophores, providing a pathway for energy dissipation. Alternatively, or in addition, changes in the chromophore upon absorption of light could influence interactions between the N- and C-terminal domains of the OCP which, by revealing new sites for interprotein interaction, could be functionally relevant. These hypotheses are discussed below in the context of analogous mechanisms in other blue-light responsive proteins.

The residues within 3.9Å of the carotenoid are shown in Fig. 4A. Of these 24 residues, eight are highly conserved aromatic amino acids (Fig. 3). All of these, except the two in the C-terminal domain that hydrogen bond to the carotenoid (Tyr^{201} and Trp^{288}), are located in the N-terminal domain where they form a dense constellation around the carotenoid. A tendency for carotenoids to be surrounded by aromatic amino acids in all structurally characterized photosynthetic pigment protein complexes has been noted. The aromatic sidechains are thought to influence selectivity for carotenoid binding (64) and the pi-pi stacking interactions provide an important noncovalent force in binding carotenoid to the protein (65). Both the orientation of the aromatic sidechains and their distance to the carotenoid have been proposed to be functionally significant (65). In the N-terminal domain of the OCP, absolutely conserved Trp^{41}, Trp^{110} and Tyr^{44} surround the terminal ring of the ECN (Fig. 4*C*). Several structural features in the N-terminal domain suggest that it may be important in intra- and or inter-protein interactions mediating the photoprotective function of the OCP. A water molecule conserved among the wildtype OCP structures (W60) and the sidechains of Tyr^{44} (which displays alternate sidechain conformations) and Trp^{41} surround one of only two regions in the OCP in which the carotenoid is solvent exposed (Fig. 4*C*). Movement of either of these sidechains, and/or of the conserved water molecule could increase surface accessibility of the carotenoid. Likewise, conserved methionine residues in this region could facilitate structural rearrangements in activation of the OCP. The SD atoms of three absolutely conserved methionine residues (83, 117, and 161) make intraprotein aromatic-sulfur interactions (66) with Trp^{41} and Trp^{110} sidechains (Fig. 4*C*). Methionine sidechains, because of their conformational flexibility are often involved in protein conformational changes or molecular recognition (67,68). Photoactivation in BLUF domains provides an example. In the BLUF domain of BlrP1(33), a conserved methionine residue undergoes a large positional displacement which changes its interaction with a glutamine (or a tryptophan in AppA; (34)) residue to accommodate the latter's movement in response to the absorption of light (33,34,69).

Characterization of *Synechocystis* OCP point mutants was used to probe the role of single amino acids in the OCP's photoprotective function. While the effect of changing these amino acids in photoconversion (from orange to red) can be monitored by

measuring the spectral change in the OCP absorbance in response to blue-green light (Fig. 1), the degree of photoprotection is measured by analyzing fluorescence quenching of mutants (Fig. 6). The OCP-related photoprotective mechanism involves an increase of energy dissipation as heat in the phycobilisome. This results in a decrease (quenching) of the phycobilisome fluorescence that can be detected a PAM fluorometer (13,70). Mutants impaired in OCP-mediated photoprotection have reduced blue-light induced quenching. To verify that any reduction in fluorescence quenching in the mutants was not the result of reduced OCP levels, a second mutation to induce the overexpression of the OCP was made in each mutant. By measuring OCP content in the overexpressing mutants we verified that the phenotypic changes observed were not due to a reduced level of the OCP in the cells (Supp. Fig 3).

Previously, we have shown that changing Trp^{110} to a serine abolishes the OCP's photoprotective function (19). To test the hypothesis that the aromatic character of the sidechain in this position is critical to function, we substituted Trp^{110} with phenylalanine. In the W110F mutant, OCP incompletely photoconverts to the red form (Fig 1). The conversion is incomplete because about 30% of the protein contained zeaxanthin and were consequently not photoactive. However, in the single and double (overexpressing) W110F mutants, the level of photoprotection was similar to the wildtype and the overexpressing wildtype strains respectively (Fig 6), confirming the importance of the role of the aromatic amino acid in this position. In the single and double W110F mutant, the OCP's photoconversion (Fig. 1) and photoprotective function (Fig. 6) are similar to wildtype, confirming the importance of the role of the aromatic amino acid in this position.

Likewise, changing Tyr^{44} to a serine results in a lack of photoconversion (Fig. 1) and fluorescence quenching (Fig. 6); however changing Tyr^{44} to another aromatic amino acid (Y44F) did not affect photoconversion or photoprotection (Figs. 1, 6). Thus, like Trp^{110}, the aromatic character of this sidechain appears to be essential to the OCP function. We crystallized the Y44S-OCP and solved the structure. Other than increased solvent accessibility to the carotenoid due to the substitution of a smaller sidechain at this position, there are no substantial differences between the structure of the Y44S mutant and the wildtype OCP. This suggests either that solvent accessibility at this site is not important to the function of the OCP, or it is the ability to modulate the accessibility to solvent that is important for function. As expected, the conserved water molecule (W60) that hydrogen bonds to the Tyr^{44} is not visible in the structure of the Y44S-OCP nor is there ordered solvent hydrogen bonding to the serine sidechain, however the resolution limit of this structure is relatively low (2.7Å). Crystallization of the Y44S mutant was more challenging than the wildtype. The wildtype and mutant OCP protein preparations were of comparable purity, possibly indicating that the lower resolution may be a result of higher overall flexibility of the Y44S mutant protein, and therefore conformational heterogeneity, in the mutant OCP.

Additional Structural Implications for Function of the OCP. In the model of the mechanism for the OCP's photoprotective function, the OCP interacts with the core of the phycobilisome. Presumably to dissipate excitation energy, the carotenoid must approach the phycobilisome core for energy transfer from its chromophores. This could also be facilitated by conformational changes in the OCP that would reversibly allow additional carotenoid exposure. This hypothesis is supported by Fourier transform infrared spectroscopy (FTIR) data that indicates that there are secondary structure changes upon photoconversion by blue light (19). Recent observations that glutaraldehyde and high concentrations of sucrose or glycerol abolish OCP mediated non-photochemical quenching in *Synechocystis* (14,71) are consistent with a role of protein motion in the OCP's photoprotective function.

Alterations in the interactions between the N- and C-terminal domain may be important in the OCP photoprotective function by serving as a means for propagating a signal or exposing sites for interprotein interactions. The interaction between the N- and C-terminal domains can be divided into two regions (Fig. 2*A* and 2*B*), we refer to as the N-terminal and the central interfaces.

The N-terminal interface between the N- and C-terminal domains buries 947 $Å^2$ and

775 Å^2 of the N- and C-terminal domains, respectively. It involves the first 19 amino acids of the N-terminal domain (which contains a short helix, αA) that extends away from the N-terminal domain to interact with the solvent-exposed face of the beta sheet and the end of the C-terminal domain (Fig. 2*B*). Many of the amino acids making up this face of the sheet and the terminal loop are absolutely conserved among OCP orthologs (Gln^{224}, Glu^{258}, Lys^{268}, Thr^{279}, Arg^{289}, Phe^{300}, Asp^{304}, Leu^{306}, Ser^{308} and Glu^{311}; Fig. 2*B*). As noted above, light absorption by the carotenoid in the OCP, and consequent alteration of the hydrogen bonding of the carotenoid to the C-terminal domain, could be propagated to the N-terminal extension (Fig. 2*B*). A paradigm for this type of signal transduction is observed in LOV domains, in which the signal emanating from the beta sheet core is propagated to a helix from a remote part of the protein that is packed against the core in the resting state. For example, in phototropin, photoactivation of the FAD chromophore alters its hydrogen bonding to the protein which is communicated through the beta sheet, culminating in the displacement of a short alpha-helix, Jα, that is associated with the LOV domain, stimulating kinase activity (72-75). The associated FTIR shift patterns during this LOV domain photoactivation are similar to those observed for activation of the OCP (19).

In the OCP, structurally conserved water molecules could also play a role in signal transduction Conserved water molecules are known to have various roles in protein structure and function (76); for example, in rhodopsin water molecules are proposed to be involved in spectral tuning and regulating activity (77). Displacement of conserved water molecules is thought to be important in effecting conformational changes in signal transduction (78-80). In the N-terminal interface there are six structurally conserved water molecules (W1, W3, W42, W76, W84, W290) in a depression on the protein surface beneath a semicircular ridge formed by interaction of the N-terminal extension and the beta sheet. W1 and W3 are partially buried and have relatively low B-factors (18.1 and 15.7 Å^2). Movement of the N-terminal extension would increase the solvent accessibility of these water molecules as well as the solvent accessibility of the conserved amino acids on this face of the beta sheet.

Alternatively, a change in the interaction of the N- and C-terminal domain of the OCP across the central interface could also be involved in the OCP's photoprotective mechanism. Given that the two domains are joined by a linker (residues 163-193) that appears to be flexible (the electron density for this region was poorly ordered in all three *Synechocystis* OCP structures described here), alterations in the conformation of the linker could result in changes in the central interface between the N- and C-terminal domains, increasing the exposure of the carotenoid for interaction with the phycobilisome.

The central interface buries 628 Å^2 and 723 Å^2 of the N- and C-terminal domains respectively. It contains eight structurally conserved water molecules (Fig. 2*B*). Two of these (W20, W125) are within 3.9 Å of the carotenoid and are found in the second region of the OCP in which the carotenoid is slightly solvent exposed. The interface is stabilized by 4 hydrogen bonds, including two formed between the pairs of conserved residues Asn^{104} and Trp^{277} and Arg^{155} and Glu^{244}. The latter salt bridge also flanks the surface depression in which the carotenoid is solvent exposed. Both Arg^{155} and Glu^{244} hydrogen bond to a structurally conserved water molecule (W200). Breakage of this salt bridge, and the concomitant movement of the sidechains, would increase the solvent accessibility of the carotenoid and of the conserved water molecules exposing new hydrogen bonding partners for other molecules. A change in the solvent accessibility of the chromophore and related rearrangements in hydrogen bonding and associated changes in electrostatic potential and shape complementarity is known to be important for the photocycle of PYP (26).

To examine the role of this interdomain salt bridge for OCP function, Arg^{155} was changed to a leucine. Upon illumination with blue-green light (400-550 nm) at 10°C, the orange His-tagged R115L-OCP (containing traces of zeaxanthin, Table 2) was completely photoconverted to the red form (Fig. 1). The spectrum of the red form of the R155L OCP was similar to that of the WT OCP. The maxima of both spectra was at 500-510 nm but the WT red OCP is slightly broader in the red region of the spectrum. However, the R155L mutant under

illumination was unable to induce fluorescence quenching (Figs. 6, 7). This indicates that photoconversion and quenching are discrete events and suggests that changes in the interaction of the N- and C-terminal domain at the central interface are critical to the structural events that allow the OCP dissipate excess energy from the phycobilisome. The 1.7 Å crystal structure of the R155L mutant revealed no significant differences from the wildtype in overall structure of the OCP (RMS deviation of 0.2 Å over the alpha carbon backbones of the dimers. A glycerol molecule necessary to the crystallization is found in the space formerly occupied by the arginine sidechain (Fig 2*C*) and hydrogen bonds (2.7Å) to the Glu^{244} side chain. The glycerol compensates for the R155L mutation and stabilizes the interface between the N- and C-terminal domains, possibly immobilizing it and so preventing conformational changes that are essential to photoprotection by the OCP.

CONCLUSIONS

The 1.65 Å crystal structure of the *Synechocystis* OCP will be valuable to ongoing genetic and spectroscopic studies of OCP-mediated photoprotection in cyanobacteria. The structural and functional characterization of the mutants reported here are the first steps toward dissecting out the roles of single amino acids and perhaps structural water molecules in the OCP's function. The mutants confirm previous hypotheses about the role of aromatic amino acids and conformational changes in signal transduction in the function of the OCP. Furthermore, the R155L mutation provides the first evidence that photoconversion and photoprotection are discrete events in the OCP's mechanism. Further studies of this mutant with Raman and Infrared spectroscopy will provide information about the carotenoid-protein interaction in solution and the changes in the protein induced by light provide key information for elucidating the precise details of the OCP's photoprotective mechanism. Likewise, efforts are underway to crystallize the photoactivated form of the OCP; this structure should reveal changes in the carotenoid and protein that underlie the spectral differences between the orange and red forms.

Signalling proteins tend to be modular and constructed by combining sensor and effector domains (81). Like other blue-light photoreceptors, the OCP is modular, and there are some similarities between its C-terminal domain and those of other blue-light sensory domains, including ligand/cofactor binding within its α/β fold. Recently it has been noted that there are parallels emerging between the mechanism of light sensing in BLUF and LOV domains; the structural basis of function of other blue-light photoreceptor proteins can be used to guide the development of new hypotheses about the mechanism of OCP function. If the OCP proves to share similar mechanisms in photoactivation and signalling it will enhance our understanding of the evolution of bacterial mechanisms to detect and respond to blue light in their environment.

REFERENCES

1. Demmig-Adams, B. (1990) *Biochim Biophys Acta* **1020**, 1-24
2. Horton, P., Ruban, A. V., and Walters, R. G. (1996) *Annual review of Plant Physiol. and plant molecular biology* **47**, 655-684
3. Muller, P., Li, x. P., and Niyogi, K. K. (2001) *Plant Physiol.* **125**, 1558-1566
4. Niyogi, K. K. (1999) *Annual review of Plant Physiol. and plant molecular biology* **50**, 333-359
5. Gilmore, A. M., and Yamamoto, H. Y. (1993) *Photosynth Res* **35**, 67-78
6. Yamamoto, H. Y. (1979) *Pure and Applied Chemistry* **51**, 639-648
7. Li, X. P., Björkman, O., Shih, C., Grossman, A. R., Rosenquist, M., Jansson, S., and Niyogi, K. K. (2000) *Nature* **403**, 391-395
8. Pascal, A. A., Liu, Z., Broess, K., van Oort, B., van Amerongen, H., Wang, C., Horton, P., Robert, B., Chang, W., and Ruban, A. (2007) *Nature* **450**, 575-578
9. Ruban, A. V., Berera, R., Ilioaia, C., van Stokkum, I. H. M., Kennis, J. T. M., Pascal, A. A., van Amerongen, H., Robert, B., Horton, P., and van Grondelle, R. (2007) *Nature* **450**, 575-578
10. Ruban, A. V., Rees, D., Pascal, A. A., and Horton, P. (1992) *Biochim Biophys Acta* **1102**, 39-44
11. El Bissati, K., Delphin, E., Murata, N., Etienne, A., and Kirilovsky, D. (2000) *Biochim Biophys Acta* **1457**, 229-242
12. Rakhimberdieva, M. G., Stadnichuk, I. N., Elanskaya, I. V., and Karapetyan, N. V. (2004) *FEBS Lett.* **574**, 85-88
13. Wilson, A., Ajlani, G., Verbavatz, J. M., Vass, I., Kerfeld, C. A., and Kirilovsky, D. (2006) *Plant Cell* **18**, 992-1007
14. Scott, M., McCollum, C., Vasil'ev, S., Crozier, C., Espie, G. S., Krol, M., Huner, N. P., and Bruce, D. (2006) *Biochemistry* **45**, 8952-8958
15. Ihalainem, J., D'Haene, S., Yeremenko, N., van Roon, H., Arteni, A., Boekema, E., van Grondelle, R., Matthijs, H. C. P., and Dekker, J. (2005) *Biochemistry* **44**, 10846-10853
16. Yeremenko, N., Kouril, R., Ihalainem, J., D'Haene, S., van Oosterwijk, N., Andrizhiyevka, E., Keegstra, W., Dekker, H., Hagemann, M., Boekema, E., Matthijs, H. C. P., and Dekker, J. (2004) *Biochemistry* **43**, 10308-10313
17. Havaux, M., Guedeney, G., He, Q., and Grossman, A. R. (2002) *Biochim Biophys Acta* **1557**, 21-33
18. Wilson, A., Boulay, C., Wilde, A., Kerfeld, C. A., and Kirilovsky, D. (2007) *Plant Cell* **19**, 656-672
19. Wilson, A., Punginelli, C., Gall, A., Bonetti, C., Alexandre, M., Routaboul, J. M., Kerfeld, C. A., van Grondelle, R., Robert, B., Kennis, J. T., and Kirilovsky, D. (2008) *Proceedings of the National Academy of Sciences of the United States of America* **105**, 12075-12080
20. Kirilovsky, D. (2007) *Photosynth Res* **93**, 7-16
21. Kerfeld, C. A., Alexandre, M., and Kirilovsky, D. (in press) The orange carotenoid protein of cyanobacteria. . in *Carotenoids: Physical, Chemical and Biological Functions and Properties (*Landrum, J. ed., CRC Press
22. Boulay, C., Abasova, L., Six, C., Vass, I., and Kirilovsky, D. (2008a) *Biochim Biophys Acta* **1777**, 1344-1354
23. Hihara, Y., Kamei, A., Kanehisa, M., Kaplan, A., and Ikeuchi, M. (2001) *Plant Cell* **13**, 793-806
24. Singh, A. K., Thanura, E., Bhattacharyya-Pakrasi, M., Aurora, R., Ghosh, B., and Pakrasi, H. B. (2008) *Plant Physiology*

148, 467-478
25. Fulda, S., Mikkat, S., Huang, F., Huckauf, J., Marin, K., Norling, B., and Hagemann, M. (2006) *Proteomics* **6**, 2733-2745
26. Genick, U. K., Borgstahl, G. E. O., Ng, K., Ren, Z., Pradervand, C., Burke, P. M., Srajer, V., Teng, T.-Y., Schildkamp, W., McRee, D. E., Moffat, K., and Getzoff, E. D. (1997) *Science (New York, N.Y* **275**, 1471-1475
27. Hellingwerf, K. J., Hendriks, J., and Gensch, T. (2003) *J. Phys. Chem. A* **107**, 1082-1094
28. Crosson, S., Rajagopal, S., and Moffat, K. (2003) *Biochemistry* **42**, 2-10
29. Losi, A., and Gartner, W. (2008) *Proc. Natl. Acad. Sci. USA* **105**, 7-8
30. Swartz, T. E., Tseng, T.-S., Frederickson, M. A., Paris, G., Comerci, D. J., Rajashekara, G., Kim, J.-G., Mudgett, M. B., Splitter, G. A., Ugalde, R. A., Goldbaum, F. A., Briggs, W. R., and Bogomolni, R. A. (2007) *Science (New York, N.Y* **317**, 1090-1093
31. Losi, A. (2004) *Photochem Photobiol* **3**, 566-574
32. Gomelsky, M., and Klug, G. (2002) *Trends in Biochemical Sciences* **27**, 497-500
33. Barends, T. R. M., Hartmann, E., Griese, J. J., Beitlich, T., Kirienko, N. V., Ryjenkov, D. A., Reinstein, J., Shoeman, R. L., Gomelsky, M., and Schlichting, I. (2009) *Nature* **459**, 1015-1018
34. Jung, A., Reinstein, J., Domratcheva, T., Shoeman, R. L., and Schlichting, I. (2006) *Journal of Molecular Biology* **362**, 717-732
35. Metz, S., Jager, A., and Klug, G. (2009) *J. Bacteriol.* **191**, 4473-4477
36. Losi, A. (2007) *Photochem Photobiol* **83**, 1283-1300
37. Möglich, A., Ayers, R. A., and Moffat, K. (2009) *Structure* **17**, 1282-1294
38. Kerfeld, C. A., Sawaya, M. R., Brahmandam, V., Cascio, D., Ho, K. K., Trevithick-Sutton, C. C., Krogmann, D. W., and Yeates, T. O. (2003) *Structure* **11**, 55-65
39. Herdman, M., Delaney, S. F., and Carr, N. G. (1973) *J. Gen. Microbiol.* **79**, 233–237
40. Yasuhiro, K., Hiroyuki, K., and Kazuhiko, S. (2001) *ELECTROPHORESIS* **22**, 1004-1007
41. Polivka, T., Kerfeld, C. A., Pascher, T., and Sundström, V. (2005) *Biochemistry* **44**, 3994-4003
42. Punginelli, C., Wilson, A., Routaboul, J.-M., and Kirilovsky, D. (2009) *Biochimica et Biophysica Acta (BBA) - Bioenergetics* **1787**, 280-288
43. Otwinowski, Z., and Minor, W. (1997) *Macromolecular Crystallography, Pt A* **276**, 307-326
44. Read, R. J. (2001) *Acta Crystallogr D Biol Crystallogr* **57**, 1373-1382
45. Collaborative Computational Project, N. (1994) *Acta Crystallogr D Biol Crystallogr* **50**, 760-763
46. Adams, P. D., Grosse-Kunstleve, R. W., Hung, L. W., Ioerger, T. R., McCoy, A. J., Moriarty, N. W., Read, R. J., Sacchettini, J. C., Sauter, N. K., and Terwilliger, T. C. (2002) *Acta Crystallogr D Biol Crystallogr* **58**, 1948-1954
47. Murshudov, G. N., Vagin, A. A., and Dodson, E. J. (1997) *Acta Crystallogr D Biol Crystallogr* **53**, 240-255
48. Emsley, P., and Cowtan, K. (2004) *Acta Crystallogr D Biol Crystallogr* **60**, 2126-2132
49. Davis, I. W., Murray, L. W., Richardson, J. S., and Richardson, D. C. (2004) *Nucleic Acids Res* **32**, W615-619
50. Kabsch, W. (1976) *Acta Crystallographica Section A* **32**, 922-923
51. Laskowski, R. A. (2009) *Nucleic Acids Research* **37**, D355-D359
52. Krissinel, E., and Henrick, K. (2007) *Journal of Molecular Biology* **372**, 774-797
53. Laskowski, R. A., Watson, J. D., and Thornton, J. M. (2005) *Nucleic Acids Research* **33**, W89-W93

54. Tina, K. G., Bhadra, R., and Srinivasan, N. (2007) *Nucleic Acids Research* **35**, W473–W476
55. Wallace, A. C., Laskowski, R. A., and Thornton, J. M. (1995) *Protein Engineering* **8**, 127-134
56. DeLano, W. L. (2002). DeLano Scientific, Palo Alto, CA
57. Jones, T. A., Zou, J. Y., Cowan, S. W., and Kjeldgaard, M. (1991) *Acta Crystallographica Section A* **47**, 110-119
58. Ponstingl, H., Henrick, K., and Thornton, J. M. (2000) *Proteins: Structure, Function, and Genetics* **41**, 47-57
59. Nakasone, Y., Eitoku, T., Matsuoka, D., Tokutomi, S., and Terazima, M. (2006) *Biophys. J.* **91**, 645-653
60. Rajagopal, S., and Vishveshwara, S. (2005) *FEBS J.* **272**, 1819-1832
61. Cleland, W. W. (2000) *Archives of Biochemistry and Biophysics* **382**, 1-5
62. Anderson, S., Crosson, S., and Moffat, K. (2004) *Acta Crystallographica* **D60**, 1008-1016
63. Burley, S. K., and Petsko, G. A. (1985) *Science (New York, N.Y* **299**, 23-28
64. Roszak, A. W., McKendrick, K., Gardiner, A. T., Mitchell, I. A., Isaacs, N. W., Cogdell, R. J., Hashimoto, H., and Frank, H. A. (2004) *Structure* **12**, 765-773
65. Mao, L., Wang, Y., and Hu, X. (2003) *J. Phys. Chem. B* **107**, 3963-3971
66. Reid, K. S. C., Lindley, P. F., and Thornton, J. M. (1985) *FEBS Letters* **190**, 209-213
67. Pal, D., and Chakrabarti, P. (2001) *J Biomol Struct Dyn.* **19**, 115-128.
68. Gellman, S. H. (2002) *Biochemistry* **30**, 6633-6636
69. Yuan, H., Anderson, S., Masuda, S., Dragnea, V., Moffat, K., and Bauer, C. (2006) *Biochemistry* **45**, 12687-12694
70. El Bissati, K., and Kirilovsky, D. (2001) *Plant Physiol.* **125**, 1988-2000
71. Rakhimberdieva, M. G., Bolychevtseva, Y. V., Elanskaya, I. V., and Karapetyan, N. V. (2007a) *FEBS Lett* **581**, 2429-2433
72. Harper, S. M., Neil, L. C., and Gardner, K. H. (2003) *Science (New York, N.Y* **301**, 1541-1544
73. Koyama, T., Iwata, T., Yamamoto, A., Sato, Y., Matsuoka, D., Tokutomi, S., and Kandori, H. (2009) *Biochemistry* **48**, 7621-7628
74. Yamamoto, A., Iwata, T., Sato, Y., Matsuoka, D., Tokutomi, S., and Kandori, H. (2009) *Biophys. J.* **96**, 2771-2778
75. Alexandre, M. T. A., van Grondelle, R., Hellingwerf, K. J., and Kennis, J. T. M. (2009) *Biophys. J.* **97**, 238-247
76. Ball, P. (2008) *Chem. Rev.* **108**, 74-108
77. Pardo, L., Deupi, X., Dölker, N., López-Rodríguez, M. L., and Campillo, M. (2007) *ChemBioChem* **8**, 19-24
78. Angel, T. E., Chance, M. R., and Palczewski, K. (2009) *Proc. Natl. Acad. Sci. USA* **106**, 8555-8560
79. Angel, T. E., Gupta, S., Jastrzebska, B., Palczewski, K., and Chance, M. R. (2009) *Proc. Natl. Acad. Sci. USA* **106**, 14367-14372
80. Hofmann, K. P., Scheerer, P., Hildebrand, P., Choe, H.-W., Park, J. H., Heck, M., and Ernst, O. (2009) *Trends in biochemical sciences* **34**, 540-552
81. Pawson, T., and Nash, P. (2003) *Science (New York, N.Y* **300**, 445-452

FOOTNOTES

Acknowledgements- We acknowledge Seth Axen for assistance in preparation of the figures for this manuscript. The carotenoid composition of the OCP was analyzed on the "Plateau Technique Spécifique de Chimie du Végétal" of IJPB. The work of AW, CP, SH and DK was supported by grants from l'Agence Nationale de la Recherche (ANR, programme CAROPROTECT), from CNRS and CEA. The work of CAK, JNK and MGK, is performed under the auspices of the US Department of Energy's Office of Science, Biological and Environmental Research Program, and by the University of California, Lawrence Berkeley National Laboratory under contract number DE-AC02-05CH11231, Lawrence Livermore National Laboratory under contract number DE-AC52-07NA27344 and the NSF (MCB-085170).

Abbreviations used are: OCP, Orange Carotenoid Protein; ECN, echinenone; NTF2, nuclear transport factor 2; RMS, root-mean-square; FTIR, Fourier transform infrared spectroscopy; TLS, Translation, Libration, Screw; LOV, Light, Oxygen or Voltage; PYP, Photoactive Yellow Protein; BLUF, Blue Light-sensing Using Flavin; HMM, Hidden Markov Model

FIGURE LEGENDS

Figure 1: Photoactivity of the isolated OCP preparations. Absorbance spectra of the dark (black) and light (red) forms of OCP isolated from the overexpressing His-tagged WT-OCP strain, from the overexpressing His-tagged W110S-OCP strain, from the overexpressing His-tagged W110F-OCP strain, from the overexpressing His-tagged Y44S-OCP strain and from the overexpressing His-tagged R155L-OCP strain and from the His-tagged WT strain. To obtain the spectrum of the red, activated form, the isolated OCP was illuminated with 1200 µmol photons m^{-2} s^{-1} of blue light, at 12°C, during 5 min.

Figure 2: Structure of the *Synechocystis* OCP. A, Stereo representation of the overall structure of the *Synechocystis* OCP. The N-terminal domain is colored blue; the C-terminal domain is shown in red and the carotenoid in sticks (orange). The linker region between the two domains is shown in gray. The sidechains of conserved residues among the OCP orthologs are shown as gray sticks with polar atoms colored (oxygen, red; nitrogen, blue; sulphur, green). Structurally conserved water molecules are shown as yellow spheres. Water molecules discussed in the text are numbered. B. The N-terminal and central interfaces between the N and C-terminal domains of the OCP, colored as in 2A. C. Structure of the central interface in the R155L OCP mutant. The glycerol molecule is shown in yellow sticks with oxygen atoms colored red.

Figure 3. Primary and secondary structure of the OCP. HMM sequence logo derived from the primary structure of OCP orthologs (reciprocal best BLAST hits to the sequence of *Synechocystis* OCP) with secondary structure elements based on the *Synechocystis* wildtype structure and colored according to Figure 2, with the exception of the N-terminal extension (purple). The linker region composed of residues 166-192. αJ is found in the *A. maxima* OCP structure, but because of disorder in this region in the *Synechocystis* OCP electron density, it was not modelled.

Figure 4. Carotenoid-protein interactions in the OCP and comparison of carotenoid conformations between *A. maxima* and *Synechocystis* OCP. A) The two molecules of *Synechocystis* wildtype OCP in the crystallographic asymmetric unit are shown. The two domains are colored as in Fig 2, and the molecule on the right contains the structurally conserved water molecules. Residues within 3.9Å of the carotenoid are shown as gray sticks with polar atoms colored as in Figure 2. Glycerol molecules are shown as yellow sticks. B). Superposition of the ECN (orange) and 3'hydroxyechinenone (blue) from the *Synechocystis* and *A. maxima* OCP structures. C) Close-up of the carotenoid-protein interactions in the N-terminal domain; sidechains and water molecules discussed in the text are labelled.

Figure 5: Gel filtration of *Synechocystis* OCP. Size exclusion chromatograms of OCP and standards (shifted up) labeled 1 for Thyroglobulin (670 kDa), 2 for γ-globulin (158 kDa), 3 for Ovalbumin (43 kDa), 4 for Myoglobin (17.6 kDa) and 5 for Bovine serum albumin (66 kDa; additional standard). OCP was eluted at 11.2 ml after ovalbumin (elution at 10.8 ml) which has a molecular weight of 43 kDa. Experiments were performed with and without OCP mixed with standards.

Figure 6: Blue-green light induced fluorescence quenching in single OCP mutants. Low light adapted cells (80µmol photons m^{-2} s^{-1}) (at 3 µg Chl mL^{-1}) of A) WT (black, closed circles), and of simple mutants Y44S (open squares blue), Y44F (closed squares blue), W110S (open triangles red), W110F (closed triangles red) and R155L (open circles green) and B) overexpressing WT-OCP (black, closed circles), W110S-OCP (open triangles red), W110F-OCP (closed triangles red), Y44S-OCP (open squares blue) and R155L-OCP (open circles green) were illuminated with high intensities (740 µmol photons m^{-2} s^{-1}) of blue-green light (400-550 nm). Fluorescence yield changes were detected with a PAM fluorometer and saturating pulses were applied to measure maximal fluorescence levels (Fm').

Table 1. X-ray data collection and refinement statistics

	Wild type	Y44S	R155L
Data collection			
Space group	$P3_2$	$P3_2$	$P3_2$
Cell dimensions			
a, *b*, *c* (Å)	82.94, 82.94, 87.63	83.19, 83.19, 87.97	82.68, 82.68, 86.57
α, β, γ (°)	90, 90, 120	90, 90, 120	90, 90, 120
Beamline	ALS 8.2.1	ALS 8.2.1	ALS 5.0.2
Wavelength	1.0000	1.0000	1.0000
Resolution (Å)	50-1.65(1.71-1.65)	50-2.65(2.74-2.65)	50-1.7(1.76-1.70)
R_{merge}	6.3(34.0)	12.9(68.7)	7.2(51.6)
I / ♦(I)	35.1(3.7)	12.0(2.1)	19.0(6.5)
Completeness (%)	99.3(93.9)	100(100)	99.0(98.1)
Redundancy	6.4(3.8)	5.6(5.3)	5.7(5.7)
Refinement			
Resolution (Å)	37.5-1.65	41.6-2.65	41.3-1.70
No. reflections	80,620	19717	71,837
R_{work} / R_{free}	16.18/19.05	19.41/25.92	15.33/19.07
No. atoms			
Protein	4667	4580	4653 8262[¥]
Water	736	150	648
ECN	82	82	82/ 190[¥]
Glycerol	12	0	42 74[¥]
Average isotropic *B*-factors (Å^2)			
Protein	26.45	35.33	24.23/ 26.17[¥]
Water	40.97	32.15	37.25
ECN	24.08	28.81	15.34/ 17.31[¥]
Glycerol	31.08	N/A	26.75[¥]/ 26.56[¥]
R.m.s deviations			
Bond lengths (Å)	0.006	0.003	0.014
Bond angles (°)	1.015	0.701	1.433

*One crystal for each structure. *Values in parentheses are for highest-resolution shell.
[¥] Includes hydrogens used in refining the pdb.

Table 2. Carotenoid Content of *Synechocystis* Wildtype (WT) and Mutant *Synechocystis* OCP

Strains*	Carotenoid[±] content (%)			Phenotype[§]
	Echinenone	OH-Echinenone	Zeaxanthin	
OverR155L	61	29	9	NoQ O/R
OverY44S	73	8	19	NoQ O
OverW110F	23	48	29	Q O/R
OverW110S	24	76	-	NoQ O
WT	5	95	-	Q O/R
OverWT	70	16	14	Q O/R

[±]See Supp. Fig. 4 for the carotenoid structures
[§]Phenotype: Q, fluorescence quenching observed; NoQ no fluorescence quenching observed; O/R, photoconverts between orange and red forms; O, does not convert to red form
*Strains: Over—denotes overexpressing strain

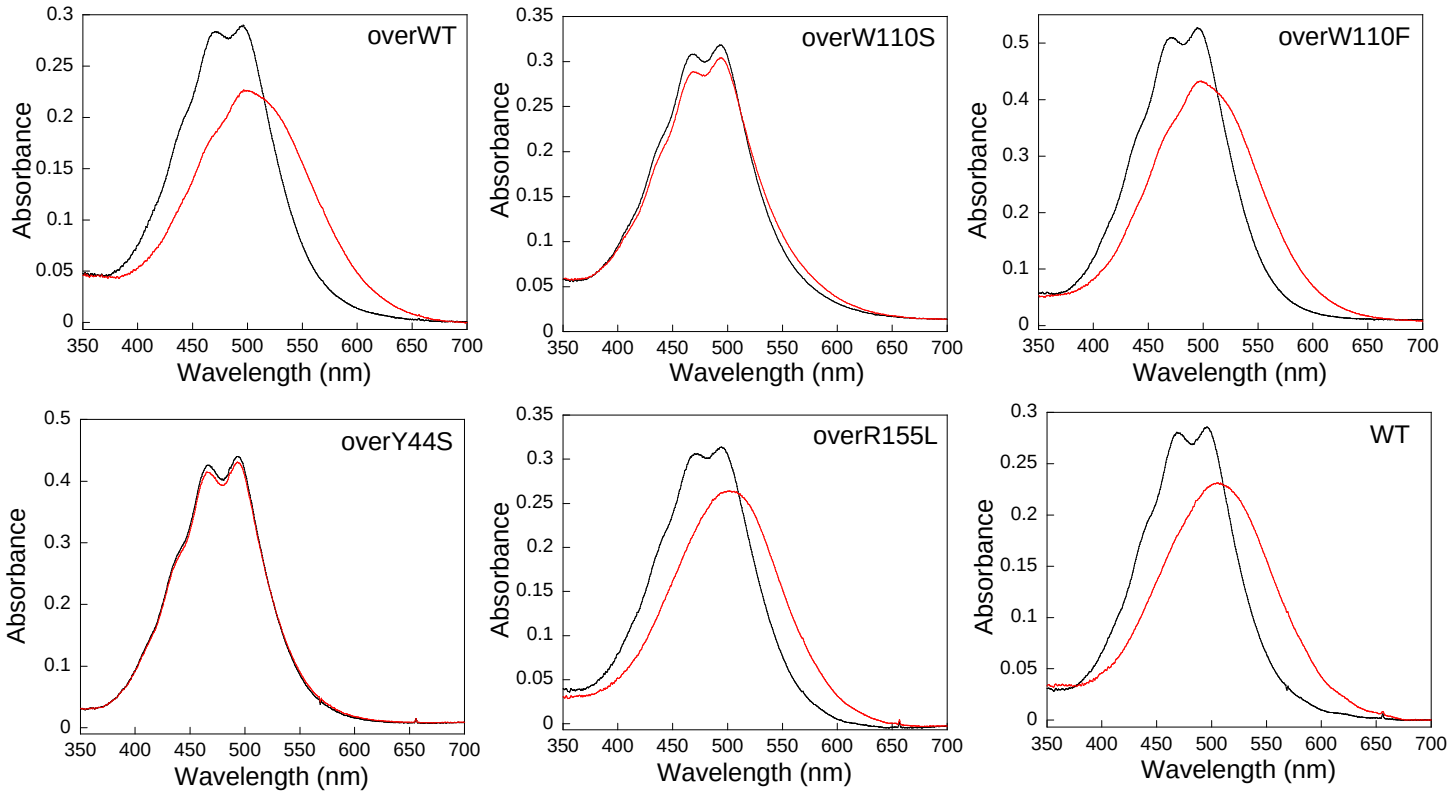
overWT
overW110S
overW110F
overY44S
overR155L
WT
Absorbance
Wavelength (nm)

Figure 1

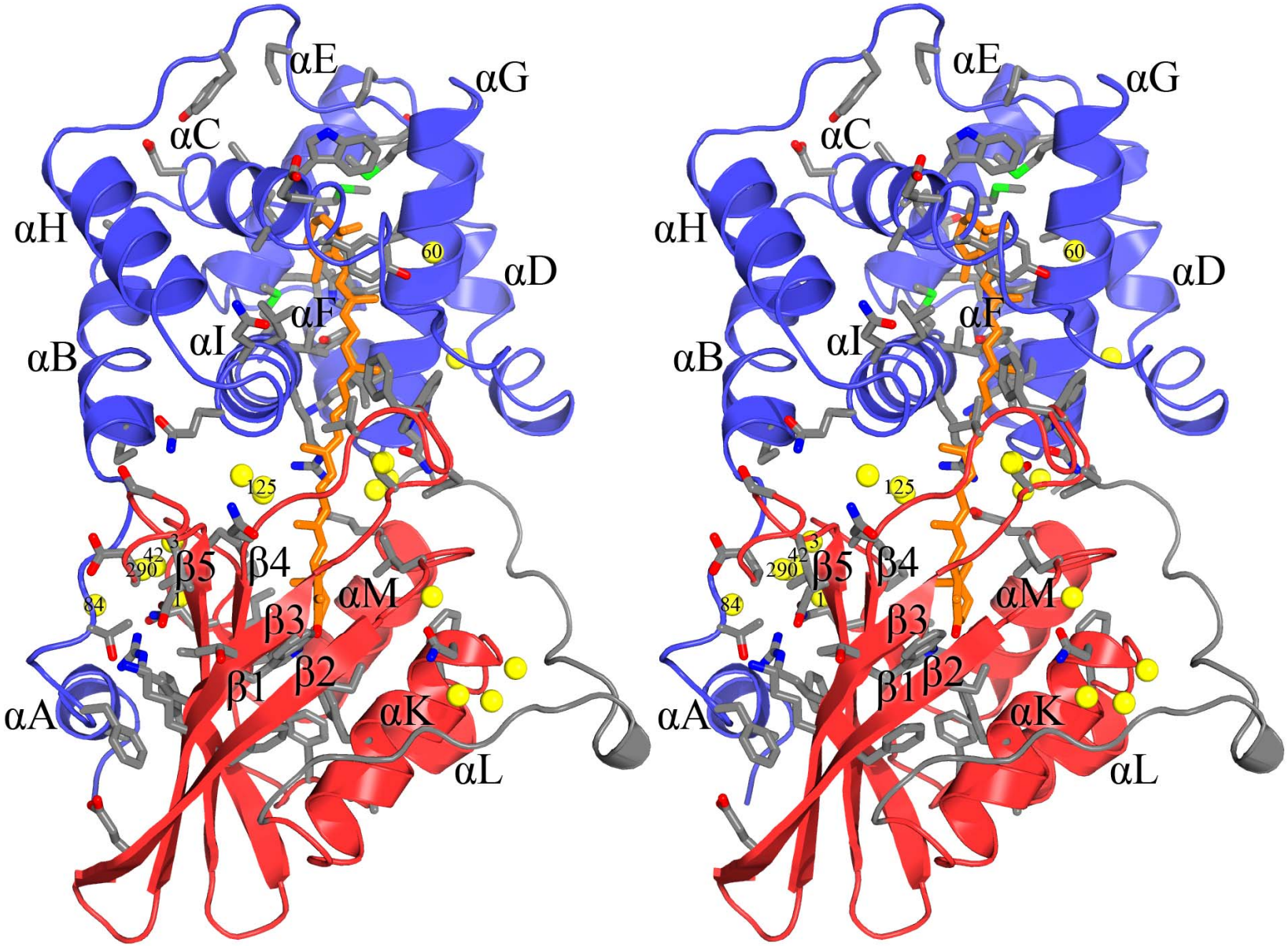
αE
αG
αC
αH
60
αD
αF
αI
αB
125
3
42
290
β5
β4
αM
84
1
β3
β1
β2
αA
αK
αL
αE
αG
αC
αH
60
αD
αF
αI
αB
125
3
42
290
β5
β4
αM
84
1
β3
β1
β2
αA
αK
αL

Figure 2A

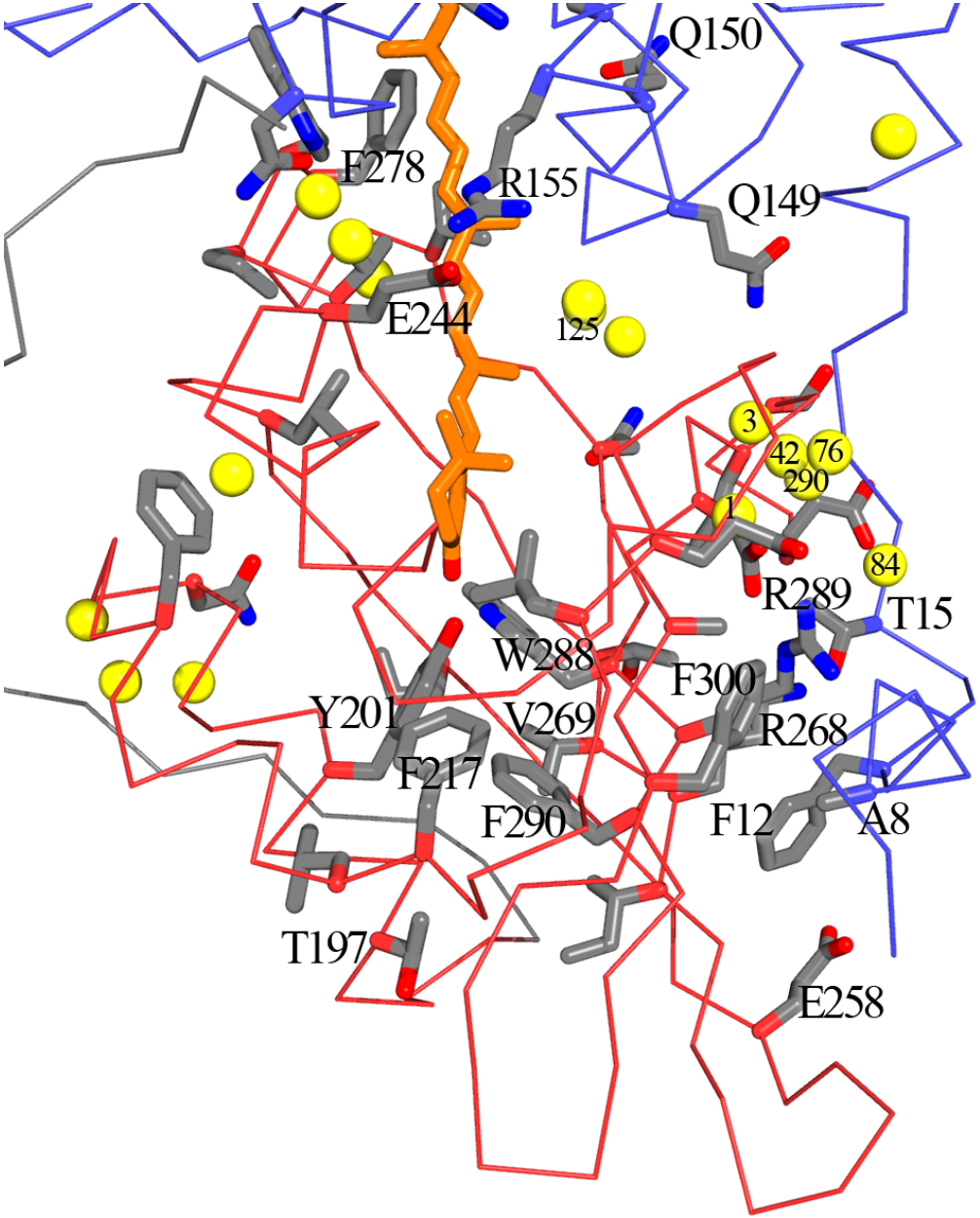
Q150
F278
R155
Q149
E244
125
3
42
76
290
1
84
R289
T15
W288
F300
Y201
V269
R268
F217
F290
F12
A8
T197
E258

Figure 2B

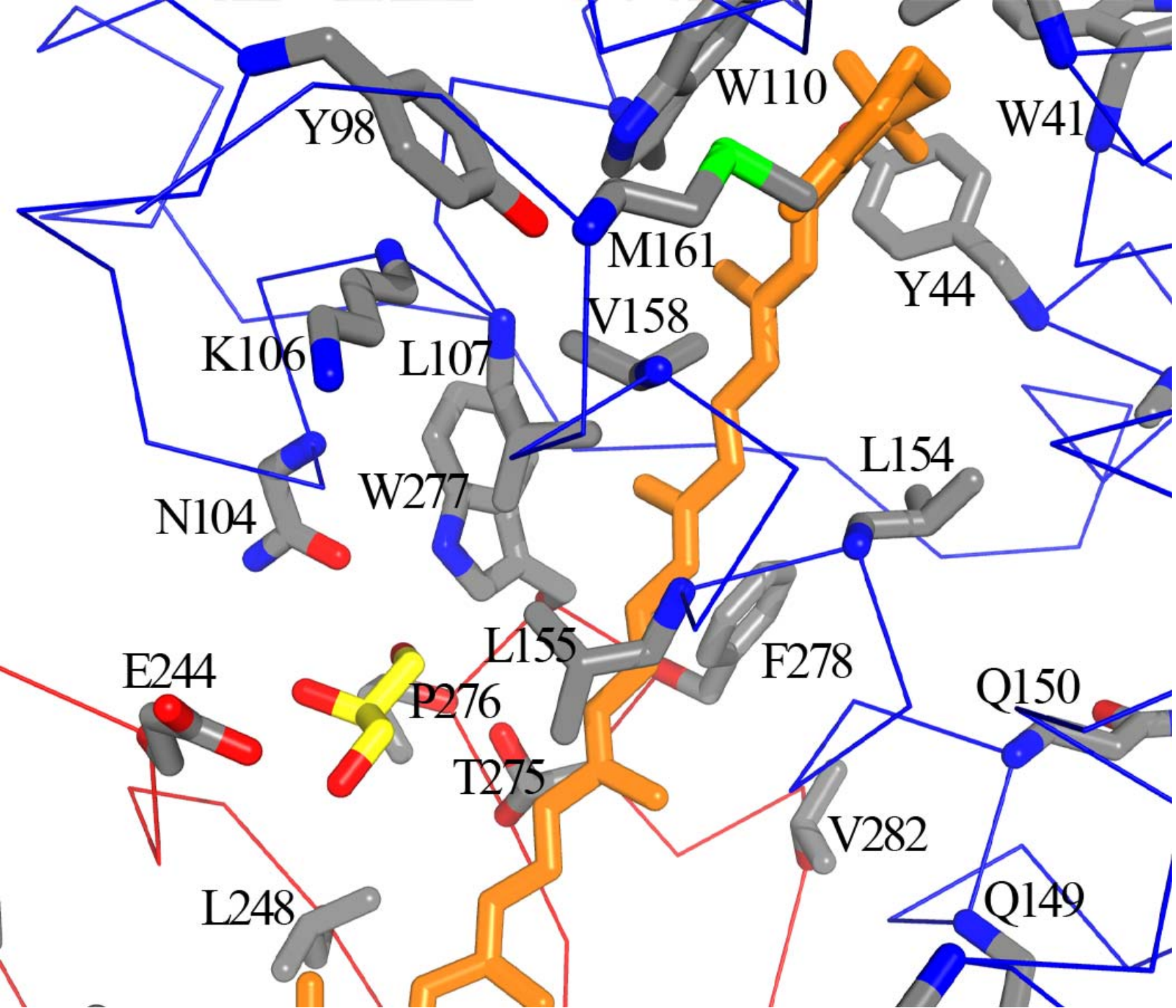
W110
W41
Y98
M161
Y44
V158
K106
L107
L154
W277
N104
L155
F278
E244
P276
Q150
T275
V282
L248
Q149

Figure 2C

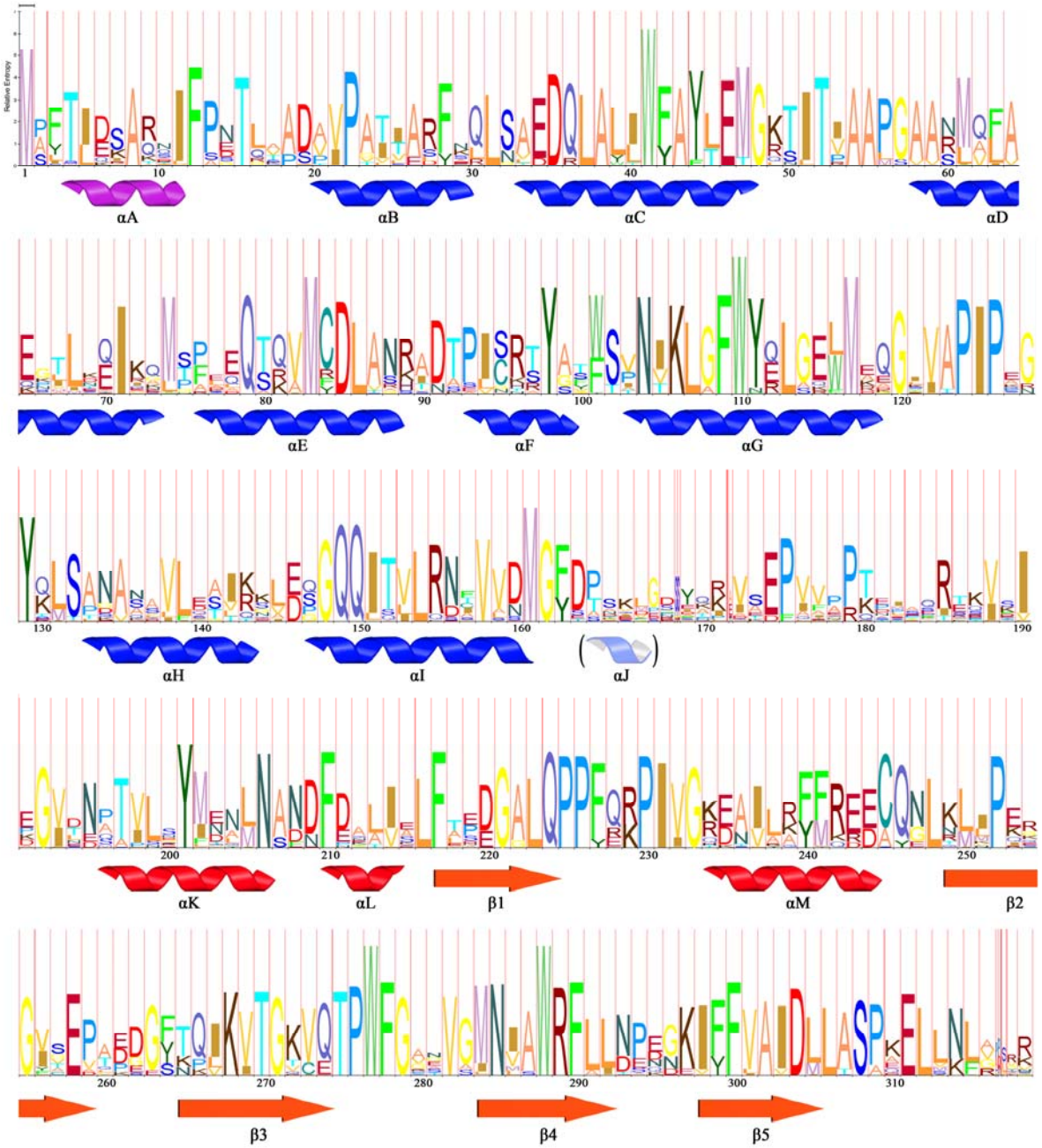
Relative Entropy
αA
αB
αC
αD
αE
αF
αG
αH
αI
αJ
αK
αL
β1
αM
β2
β3
β4
β5

Figure 3

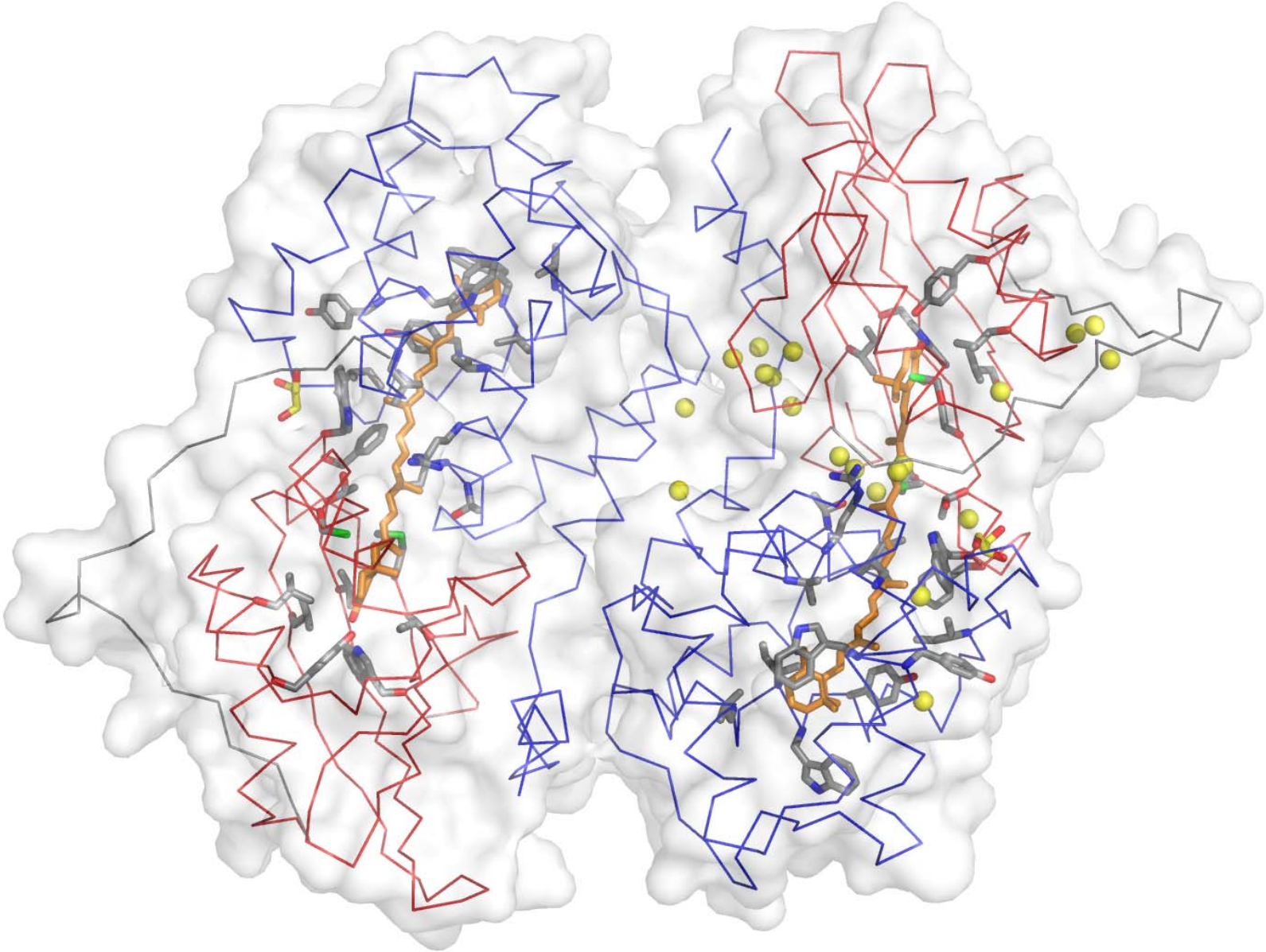

Figure 4A

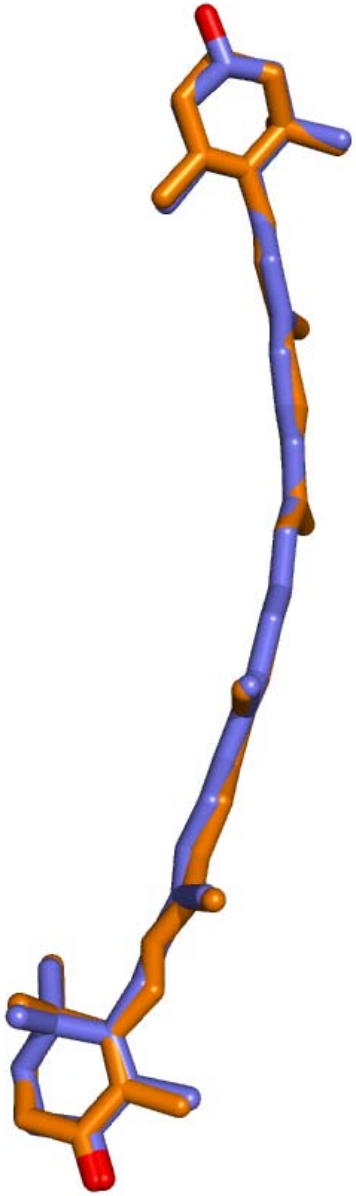

Figure 4B

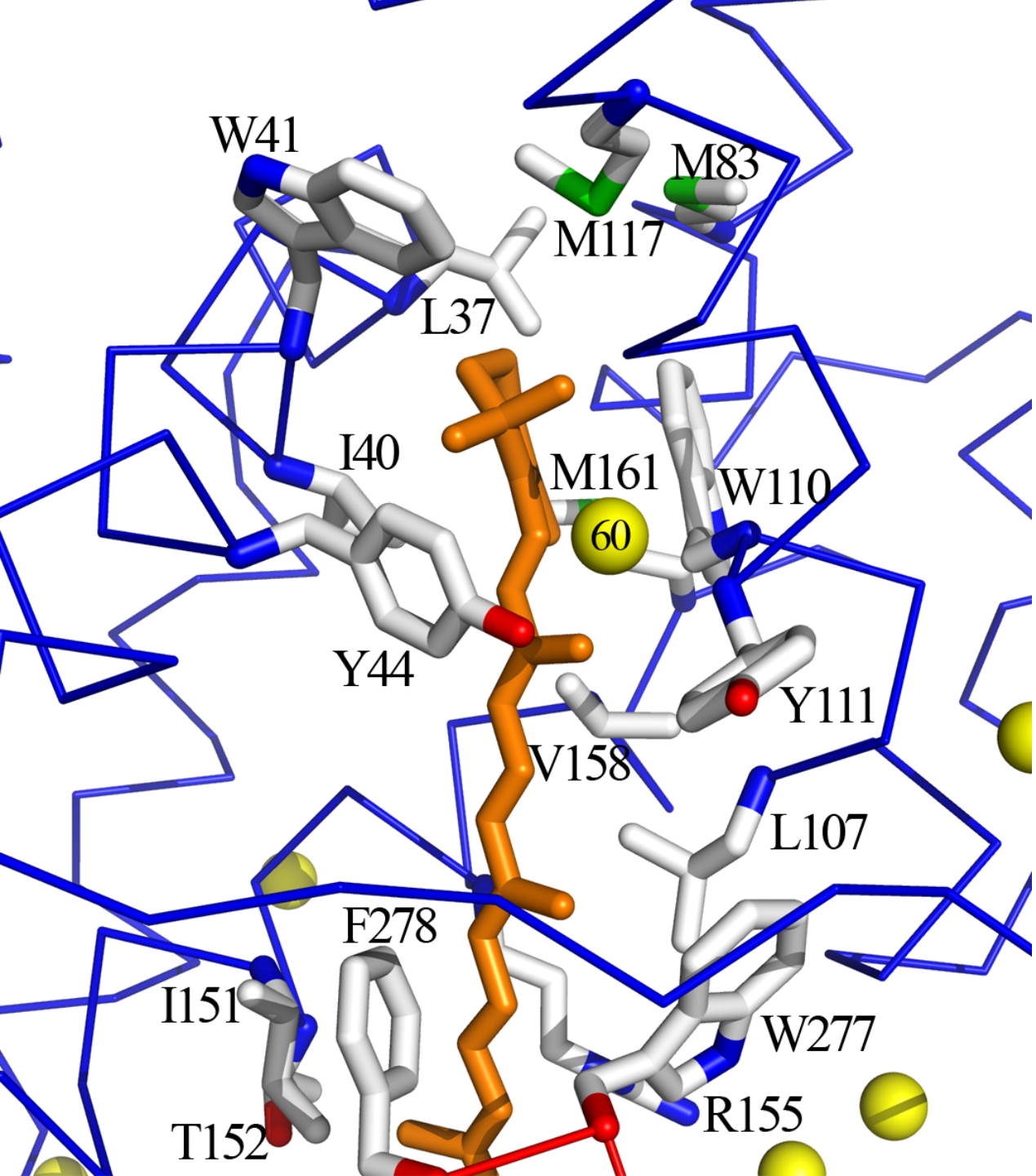
W41
M83
M117
L37
I40
M161
W110
60
Y44
Y111
V158
L107
F278
I151
W277
R155
T152

Figure 4C

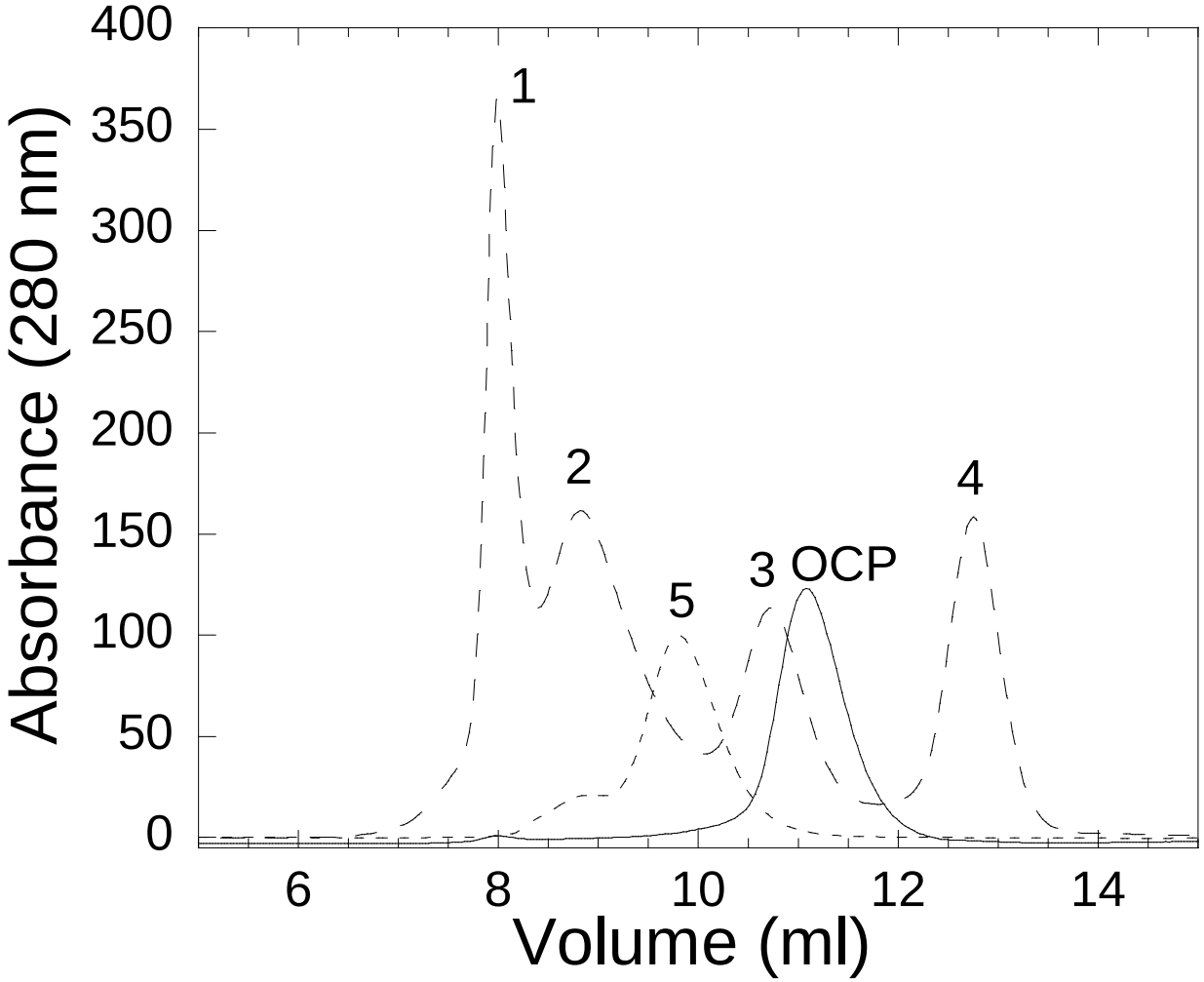
400
350
300
250
200
150
100
50
0
Absorbance (280 nm)
1
2
5
3 OCP
4
6
8
10
12
14
Volume (ml)

Figure 5

A

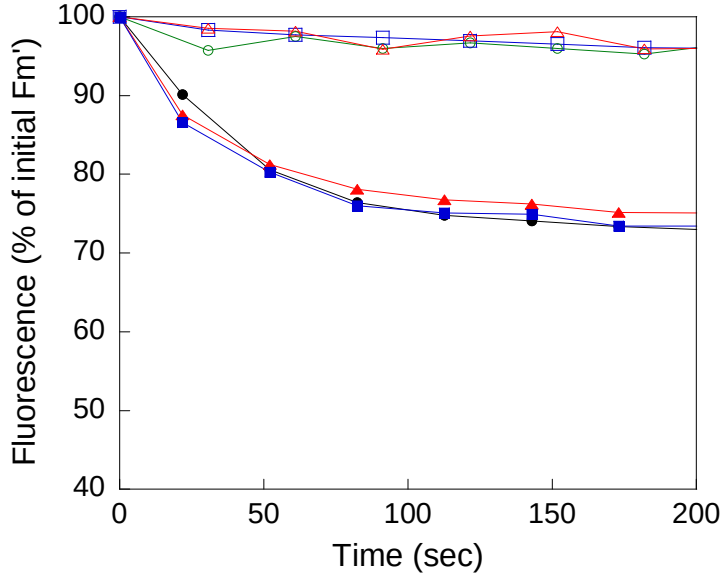
100
90
80
70
60
50
40
0
50
100
150
200
Fluorescence (% of initial Fm')
Time (sec)

B

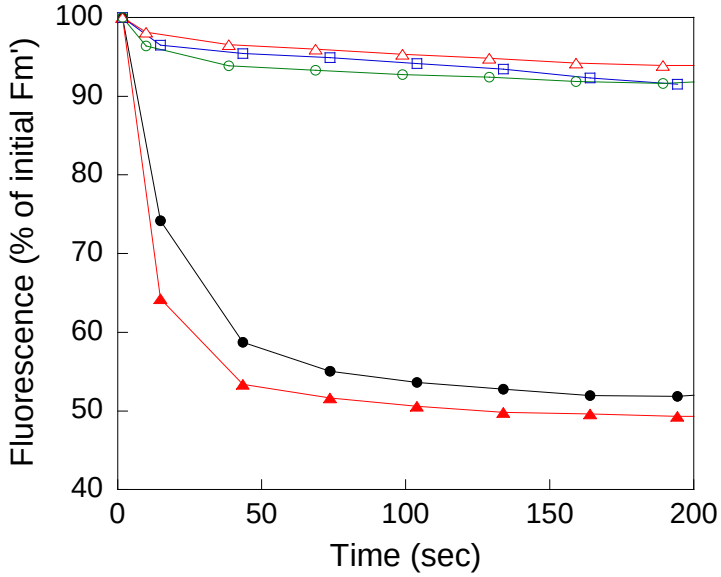
100
90
80
70
60
50
40
0
50
100
150
200
Fluorescence (% of initial Fm')
Time (sec)

Figure 6